Gibbs Phenomenon in Structural Control

H. Baruh* and S. S. K. Tadikonda†
Rutgers University, New Brunswick, New Jersey 08903

The existence of the Gibbs effect during control of flexible structures is investigated. It is shown that, due either to the choice of the actuation mechanisms as point or piecewise-continuous components or to the time history of the external excitation, discontinuities may exist in the spatial and temporal profiles of the control input. A spatial eigenfunction expansion of the control profile and a Fourier series expansion of the temporal behavior indicate the Gibbs effect. The existence of a Gibbs effect results in the excitation of the residual dynamics with higher amplitudes and in the generation of undesirable motion. The extent to which discrete actuation mechanisms such as point forces, piecewise-continuous forces, and point torquers excite the residual dynamics is compared.

I. Introduction

THIS paper is concerned with the existence of the Gibbs effect when controlling the motion of flexible structures. It is often desirable to control only part of the motion without exciting the remainder. Typical examples are large-angle maneuvers of robot arms or of spacecraft, where the maneuver forces and torques should be selected so that they excite the elastic motion as little as possible. In order not to excite the elastic motion, both the spatial and temporal distributions of the control input must be designed as continuous functions. In this paper we show that discontinuities in the spatial or temporal distribution of the control lead to a Gibbs effect in the expansion of these distributions and result in excitation of undesired motion.

The best-known occurrence of the Gibbs effect is in the Fourier or any orthogonal series expansion of a function that has discontinuities in its domain or at its boundaries.[1-3] The rate of convergence of a Fourier series depends on how many times the function can be differentiated. In the neighborhood of a discontinuity the rate of convergence becomes nonuniform, a phenomenon known as the Gibbs effect.[3] If a function is k times differentiable, the coefficients in its Fourier series (or eigenfunction) expansion are $\mathcal{O}(1/r^{k+1})$, in which r is the index of expansion.

The Gibbs effect can also be found in structural mechanics problems, when approximate solutions to boundary-value problems are sought by series expansions.[4,5] In this paper we show how the Gibbs effect arises in structural control problems and analyze the consequences of the Gibbs effect on the performance of the control and on the response.

Ideally, one would like to use spatially continuously distributed actuation mechanisms. However, the current state of the art permits only discrete measurements and controllers. The relationship between using discrete controllers and the principles of structural mechanics is analyzed in Ref. 6. We demonstrate in this paper that, if point or piecewise-continuous actuation mechanisms are used, a Gibbs effect exists in the spatial distribution of the force input. When the temporal distribution of the control profile has discontinuities, the Gibbs effect is observed in the Fourier series expansion of the time dependence of the control. We show that when the Gibbs effect is present undesirable motion is excited and unnecessary work is done by the actuators, thus reducing the effectiveness of the control. We also provide guidelines for the selection of control profiles in order to minimize the consequences of the Gibbs effect.

Received June 23, 1989; presented as Paper 89-3485 at the AIAA Guidance, Navigation, and Control Conference, Boston, MA, Aug. 14-16, 1989; revision received Nov. 27, 1989.

*Associate Professor, Department of Mechanical and Aerospace Engineering. Member AIAA.

†Graduate Assistant, Department of Mechanical and Aerospace Engineering; currently, Staff Scientist, Dynacs Engineering, Palm Harbor, FL.

II. Closed-Loop Equations of Motion

Consider a one-dimensional flexible structure, whose evolution in time is described in the form

$$Lu(x,t) + m(x)\ddot{u}(x,t) = f(x,t), \qquad 0 < x < L \tag{1}$$

where $u(x,t)$ is the deformation at spatial coordinate x at time t, $m(x)$ is the mass distribution, L is a linear differential stiffness operator of order $2p$, and $f(x,t)$ is the excitation, including controls. The stiffness operator L has the general form

$$L = h_0(x) + \frac{\partial}{\partial x}\left[h_1(x)\frac{\partial}{\partial x}\right] + \cdots + \frac{\partial^p}{\partial x^p}\left[h_p(x)\frac{\partial^p}{\partial x^p}\right] \tag{2}$$

where $h_0(x)$, $h_1(x)$,..., $h_p(x)$ are algebraic functions. For example, for a beam, $p = 2$, and $h_0(x)$ corresponds to a continuously distributed linear spring, $h_1(x)$ corresponds to a distributed torsional spring or an axial force, and $h_2(x)$ denotes the beam stiffness.

The eigensolution consists of eigenvalues λ_r and associated eigenfunctions $\phi_r(x)$, which can be normalized to yield $[\phi_r(x), m(x)\phi_s(x)] = \delta_{rs}$, $[\phi_r(x), L\phi_s(x)] = \lambda_r\delta_{rs} = \omega_r^2\delta_{rs}$ ($r,s = 1,2,...$), where $(a,b) = \int ab\, dx$ and ω_r are the natural frequencies. The modal equations have the form

$$\ddot{u}_r(t) + \omega_r^2 u_r(t) = f_r(t), \qquad r = 1,2,... \tag{3}$$

in which $u_r(t)$ are modal coordinates and $f_r(t)$ modal forces. They are related to $u(x,t)$ and $f(x,t)$ by

$$u(x,t) = \sum_{r=1}^{\infty} \phi_r(x)u_r(t) \tag{4a}$$

$$u_r(t) = (u(x,t), m(x)\phi_r(x)) \tag{4b}$$

$$f(x,t) = \sum_{r=1}^{\infty} m(x)\phi_r(x)f_r(t) \tag{4c}$$

$$f_r(t) = (f(x,t), \phi_r(x)) \tag{4d}$$

where $r = 1,2,...$ and where we observe that $u_r(t)$ is the eigen-

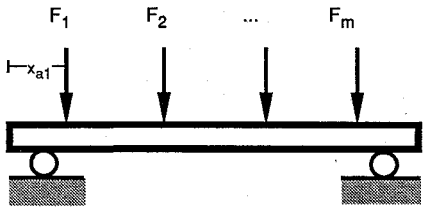

Fig. 1 Point force controller.

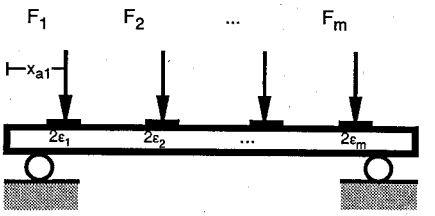

Fig. 2 Piecewise-continuous force controller.

function expansion of $u(x,t)$ and $f_r(t)$ is the eigenfunction expansion of $f(x,t)/m(x)$.

We will consider three types of discrete actuators: point force actuators, piecewise continuous force actuators, and point torquers. For point force actuators at locations x_{ai} $(i = 1,2,...,m)$, where m is the number of actuators, one can express the force profile as

$$f(x,t) = \sum_{i=1}^{m} F_i(t)\delta(x - x_{ai}) \tag{5}$$

in which $F_i(t)$ are the actuator inputs (Fig. 1). The modal forces become

$$f_r(t) = \sum_{i=1}^{m} \int_0^L F_i(t)\delta(x - x_{ai})\phi_r(x)\,dx = \sum_{i=1}^{m} B_{ri}F_i(t), \qquad r = 1,2,... \tag{6}$$

where $B_{ri} = \phi_r(x_{ai})$.

Next consider control forces that are piecewise continuous, as shown in Fig. 2. The contact length for each actuator is $2\varepsilon_i$, with the midpoint located at x_{ai} $(i = 1,2,...,m)$. Each actuator imparts a total force of $F_i(t)$ $(i = 1,2,...,m)$. The force distribution can then be expressed as

$$f(x,t) = \sum_{i=1}^{m} \frac{F_i(t)}{2\varepsilon_i}[u(x - x_{ai} + \varepsilon_i) - u(x - x_{ai} - \varepsilon_i)] \tag{7}$$

where u is the unit step function. We observe that $f(x,t)$ is now a piecewise-continuous function and that $F_i(t)/2\varepsilon_i$ denotes the force density of the ith actuator. It follows that

$$f_r(t) = \sum_{i=1}^{m} \int_0^L \frac{F_i(t)}{2\varepsilon_i}[u(x - x_{ai} + \varepsilon_i) - u(x - x_{ai} - \varepsilon_i)]\phi_r(x)\,dx = \sum_{i=1}^{m} B_{ri}F_i(t), \qquad r = 1,2,... \tag{8}$$

where

$$B_{ri} = \frac{1}{2\varepsilon_i}\int_{x_{ai}-\varepsilon_i}^{x_{ai}+\varepsilon_i} \phi_r(x)\,dx \tag{9}$$

For point torquers located at x_{ti} $(i = 1,2,...,m)$, one can express the external excitation as[7]

$$f(x,t) = -\frac{\partial \bar{m}(x,t)}{\partial x} = \sum_{i=1}^{m} -M_i(t)\delta'(x - x_{ti}) \tag{10}$$

in which $\bar{m}(x,t)$ is the spatial torque distribution, $M_i(t)$ denotes the amplitudes of the torque inputs of actuators located at x_{ti} $(i = 1,2,...,m)$, and δ' is the spatial derivative of the Dirac delta function.[8] Substitution of Eq. (10) into the expansion theorem [Eqs. (4)] yields

$$f_r(t) = \sum_{i=1}^{m} \int_0^L -M_i(t)\delta'(x - x_{ti})\phi_r(x)\,dx = \sum_{i=1}^{m} B_{ri}M_i(t), \qquad r = 1,2,... \tag{11}$$

where

$$B_{ri} = \int_0^L -\delta'(x - x_{ti})\phi_r(x)\,dx = \phi_r'(x_{ti}) \tag{12}$$

The modal equations can be written in vector form as

$$\ddot{\boldsymbol{u}}(t) + \Lambda \boldsymbol{u}(t) = \boldsymbol{f}(t) = B\boldsymbol{F}(t) \tag{13}$$

where $\boldsymbol{u}(t)$ and $\boldsymbol{f}(t)$ are infinite-dimensional vectors containing the modal coordinates and modal vectors, Λ is a diagonal matrix containing the eigenvalues, $\boldsymbol{F}(t)$ contains the actuator (force or torque) inputs, and B is the actuator influence matrix.

III. Gibbs Effect in Fourier Series and Eigenfunction Expansions

In this section we briefly describe Fourier series and eigenfunction expansions and associated convergence issues. Given a function $f(x)$ between 0 and 2π, its Fourier series expansion is given by the periodic function $g(x)$, so that

$$g(x) = b_0 + \sum_{r=1}^{\infty} (a_r \sin rx + b_r \cos rx) \tag{14}$$

where the coefficients a_r and b_r can be found from [1-3]

$$a_r = \frac{1}{\pi}\int_0^{2\pi} f(x)\sin rx\,dx \tag{15a}$$

$$b_r = \frac{1}{\pi}\int_0^{2\pi} f(x)\cos rx\,dx \tag{15b}$$

It can be shown[3] that if $f(x)$ is piecewise continuous and has bounded total variation,

$$g(x) = \tfrac{1}{2}[f(x^+) + f(x^-)], \qquad 0 < x < 2\pi \tag{16}$$

We would like to examine the convergence of Fourier series in the neighborhood of a discontinuity. Denoting by $g_n(x)$ the nth order expansion, and by x_0 the point of discontinuity in $f(x)$, one can show that as $n \to \infty$ (Ref. 3),

$$g_n(x) - \tfrac{1}{2}[f(x_0^+) + f(x_0^-)] = \mathcal{O}(1) \tag{17}$$

which implies that convergence of $g_n(x)$ to $f(x)$ is not uniform in the neighborhood of a discontinuity. This nonuniformity in convergence is known as the Gibbs effect, and it results in oscillations and an overshoot in the plots of $g_n(x)$ in the neighborhood of the discontinuity. One can quantify the amount of overshoot for a given function.[3]

To examine amplitudes of the coefficients, consider a Fourier sine series. If $f(x)$ has continuous derivatives up to order $k-1$, one can integrate Eq. (15a) by parts k times to obtain for the rth term in the expansion

$$a_r = \frac{1}{\pi}\int_0^{2\pi} f(x)\sin rx\,dx = \frac{1}{\pi r}\int_0^{2\pi} f'(x)\cos rx\,dx = \cdots = \frac{1}{\pi(-1)^{(k/2)}r^k}\int_0^{2\pi} f^{(k)}(x)\sin rx\,dx, \qquad r = 1,2,... \tag{18}$$

where, without loss of generality, we have assumed that $f(x)$ and its even derivatives vanish at $x = 0$ and $x = 2\pi$, and k is even. If k is odd, there will be a cosine term in the integrand. It is clear that the order of the coefficients in the Fourier series depends on how many times the function $f(x)$ is differentiable. If $f(x)$ is $k-1$ times differentiable and $f^{(k)}$ is integrable, then the coefficients $a_r = \mathcal{O}(1/r^k)$. Also, since $n \to \infty$ at a point away from a discontinuity x_0 in $f^{(k-1)}(x)$, we have[3]

$$g_n(x) - f(x) = \mathcal{O}(1/n^k) \tag{19}$$

and in the neighborhood of the discontinuity,

$$g_n(x) - \tfrac{1}{2}[f(x_0^+) + f(x_0^-)] = \mathcal{O}(1/n^{k-1}) \tag{20}$$

indicating the Gibbs effect in the expansion of $f^{(k-1)}(x)$.

To extend the preceding results to eigenfunction expansions, we consider a function $f(x)$ in $[0,L]$, which is $2p$ times differentiable, and expand it in terms of the eigenfunctions $\phi_r(x)$ $(r = 1,2,...)$ associated with Eq. (1) as

$$f(x) = \sum_{r=1}^{\infty} a_r \phi_r(x) \tag{21a}$$

$$a_r = \int_0^L f(x) m(x) \phi_r(x)\, dx \tag{21b}$$

The eigenvalue problem can be expressed in terms of the eigenfunctions as

$$L\phi_r(x) = \lambda_r m(x) \phi_r(x), \qquad r = 1,2,... \tag{22}$$

Considering Eq. (22) and substituting for $m(x)\phi_r(x)$ in Eq. (21b), we obtain[3]

$$a_r = \frac{1}{\lambda_r} \int_0^L f(x) L\phi_r(x)\, dx, \qquad r = 1,2,... \tag{23}$$

Integrating Eq. (23) by parts $2p$ times yields

$$\begin{aligned} a_r = \frac{1}{\lambda_r} \Big\{ & f(x) h_1(x) \phi_r'(x) - f'(x) h_1(x) \phi_r(x) \\ & + f(x) \frac{d}{dx}[h_2(x)\phi_r''(x)] - f'(x) h_2(x) \phi_r''(x) \\ & + f''(x) h_2(x) \phi_r'(x) - \phi_r(x) \frac{d}{dx}[h_2(x) f''(x)] + \cdots \\ & - \phi_r(x) \frac{d^{p-1}}{dx^{p-1}}[h_p(x) f^{(p)}(x)] \Big\} \Big|_0^L \\ & + \frac{1}{\lambda_r} \int_0^L \phi_r(x) L f(x)\, dx, \qquad r = 1,2,... \end{aligned} \tag{24}$$

It is shown in Ref. 3 that the last term in Eq. (24) is $\mathcal{O}(1/\lambda_r)$ or lower. To investigate the Gibbs effect, we generalize the results in Ref. 10 with respect to the asymptotic behavior of the eigensolution of self-adjoint boundary-value problems to the following. As $r \to \infty$, the asymptotic behavior of the eigensolutions is governed by

$$\lambda_r \sim Cr^{2p}, \qquad \phi_r(x) \sim f(Drx), \qquad r = 1,2,... \tag{25}$$

in which the constants C and D depend on $h_p(x)$ and $m(x)$. When $p = 1$, such as in the wave equation, $f(Drx) = A_r \sin(Drx) + B_r \cos(Drx)$, and when $p = 2$, such as in the beam equation, $f(Drx) = A_r \sin(Drx) + B_r \cos(Drx) + A_r' \sinh(Drx) + B_r' \cosh(Drx)$.

Consider, for example, a uniform simply supported beam. The eigenfunctions $\phi_r(x)$ satisfy the boundary conditions $\phi_r(0) = 0$, $\phi_r(L) = 0$, $\phi_r''(0) = 0$, and $\phi_r''(L) = 0$. If we expand a continuous function $f(x)$ satisfying $f(L) = 0$, $f''(0) = 0$, $f''(L) = 0$, but $f(0) \neq 0$, we obtain from Eq. (24)

$$\begin{aligned} a_r = \frac{-1}{\lambda_r} \Big\{ & f(0) h_1(0) \phi_r'(0) \\ & + f(x) \frac{d}{dx}[h_2(x)\phi_r''(x)]\big|_{x=0} \Big\} + \mathcal{O}\left(\frac{1}{\lambda_r}\right) \end{aligned} \tag{26}$$

Considering the asymptotic behavior of the eigensolution given in Eq. (25), we have

$$a_r = \mathcal{O}\left(\frac{1}{r^4} r\right) + \mathcal{O}\left(\frac{1}{r^4} r^3\right) + \mathcal{O}\left(\frac{1}{\lambda_r}\right) = \mathcal{O}\left(\frac{1}{r}\right) \tag{27}$$

Hence, existence of the Gibbs effect is obvious.

IV. Gibbs Effect in Structural Control

In this section we demonstrate the Gibbs effect in structural control systems. This effect is observed in two areas: in the expansion of the external excitation spatially using the system eigenfunctions and in the expansion of the control input temporally by Fourier series. We first analyze the spatial distribution of the control inputs.

Consider first point force actuators. Because $f(x,t)$, as given by Eq. (5), cannot be evaluated or differentiated and its integral over x is only piecewise continuous, the modal forces $f_r(t)$ are $\mathcal{O}(1)$ for all values of r. This is another way of arriving at a well-known result: when point actuators are used, all of the modes, whether controlled or residual, receive the same order of excitation.[9]

When piecewise-continuous force actuators are used, the expression for $f(x,t)$ in Eq. (7) cannot be differentiated, but its integral over x is continuous. We conclude that for piecewise-continuous force controllers the modal inputs $f_r(t)$ are $\mathcal{O}(1/r)$. That is, the higher modes receive less excitation than the lower modes, a phenomenon that is also observed when the results of Ref. 11 are examined. From the point of view of modal control, this is a more desirable modal distribution than point forces; the residual dynamics is excited less by virtue of decreasing amplitudes of the modal excitation. For decentralized control laws, supplying the higher modes with less control is not a drawback either; the higher modes need less control in any extent, because more structural damping is present in them. In addition, piecewise-continuous actuators reduce the stress levels in the vicinity of the actuators.

Consider a uniform pinned-pinned beam with mass density ρ, whose normalized eigenfunctions can be shown to be $\phi_r(x) = \sqrt{2/\rho L} \sin(r\pi x/L)$ $(r = 1,2,...)$. With discrete force actuators located at x_{ai} $(i = 1,2,...,m)$, from Eq. (6), the modal forces are given by

$$f_r(t) = \sqrt{\frac{2}{\rho L}} \sum_{i=1}^{m} F_i(t) \sin \frac{r\pi x_{ai}}{L} \tag{28}$$

If piecewise-continuous actuators with finite contact lengths of $2\varepsilon_i = 2\varepsilon$ $(i = 1,2,...,m)$ are used, the modal forces become

$$\begin{aligned} f_r(t) &= \sqrt{\frac{2}{\rho L}} \sum_{i=1}^{m} \frac{F_i(t)}{2\varepsilon} \int_{x_{ai}-\varepsilon}^{x_{ai}+\varepsilon} \sin \frac{r\pi x}{L}\, dx \\ &= \frac{L}{r\pi\varepsilon} \sin \frac{r\pi\varepsilon}{L} \sqrt{\frac{2}{\rho L}} \sum_{i=1}^{m} F_i(t) \sin \frac{r\pi x_{ai}}{L}, \qquad r = 1,2,... \end{aligned} \tag{29}$$

We observe that the modal forces associated with the piecewise-continuous controllers can be obtained by multiplying the modal forces associated with the point controllers by

$$\frac{L}{r\pi\varepsilon} \sin \frac{r\pi\varepsilon}{L} \tag{30}$$

a clear indication that the modal forces receive lower amounts

of excitation as the contact lengths of the actuators are increased and as the mode number gets higher.

It should be noted that actuators that are currently available are actually piecewise continuous, even though the contact length of each actuator is very small. The implication is that, because control spillover has been investigated for only point actuators, a mathematical idealization, it has been analyzed for the worst case, and that it is not as critical a problem when piecewise-continuous actuators are used.

For point torquers, because the modal forces depend on the first derivatives of the eigenfunctions, the modal forces $f_r(t)$ are of order $\mathcal{O}(r)$. This feature makes point torquers less desirable than point forces if one wishes to minimize the energy in the residual dynamics. When piecewise-continuous torque actuators are considered, which is the case with the currently available hardware, the modal inputs will be $\mathcal{O}(1)$, thus exciting the residual dynamics less.

We conclude that the actuators that impart the control forces and moments to a structure should be selected as continuous as possible, and force inputs should be used instead of torque actuators. The state of the art is not yet ready to have spatially continuously distributed controllers, but some inroads are being made through magnetic-piezoelectric devices (e.g., Ref. 12). Note that one way of making a force or torque profile more continuous is to increase the number of actuators. We will demonstrate this point in the next section.

To illustrate the Gibbs effect in the temporal distribution of the loading, consider a structure that admits rigid-body modes. If our objective is to control the rigid-body motion, the control inputs should be designed so that the elastic motion is excited as little as possible.

Because $F_i(t)$ appears in every modal force expression, the Fourier series expansion of $F_i(t)$ and the Gibbs phenomenon associated with it affect each mode the same way. Our objective then becomes to select a control profile that has the lowest amplitudes in its Fourier series expansion. However, if the control inputs are periodic, such as those that move a robot arm repeatedly from one point to another or for maneuvering a spacecraft, the period of motion also affects the way the modal coordinates are excited. To analyze these effects, we will not only consider the order of the terms in the expansion of $F_i(t)$ but also the response of the modal coordinates.

The response of an elastic mode, considering zero initial conditions, is

$$u_r(t) = \frac{1}{\omega_r}\int_0^t f_r(\tau)\,\sin\omega_r(t-\tau)\,d\tau = \frac{1}{\omega_r}\sum_{i=1}^{m} B_{ri}\int_0^t F_i(\tau)\,\sin\omega_r(t-\tau)\,d\tau, \quad r = 1,2,.., \tag{31}$$

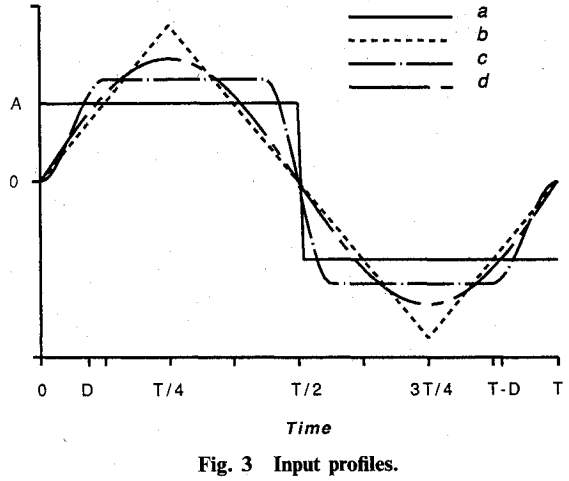

Fig. 3 Input profiles.

Assume a rest-to-rest maneuver of a rigid-body mode using a single controller; that is, replace $F_i(t)$ in Eq. (31) with $F(t)$ and B_{ri} with B_r. The maneuver is carried out as an open-loop control.

We consider a number of input profiles and compare the response and energy levels for different natural frequencies and periods of maneuvers. The input profiles are given in Fig. 3. The amplitude of each input is selected so that $F(t)$ integrated twice,

$$\int_0^T\int_0^t F(\tau)\,d\tau\,dt \tag{32}$$

has the same value in each profile, and T is the final time. This implies that, when the inputs are applied to a rigid body, the final orientation/position of the body at $t = T$ will be the same for each input configuration. The amplitudes of these profiles can be shown to be A, $2A$, $AT^2/(T-D)^2$, and $\pi A/2$ for the profiles a, b, c, and d, respectively.

As can be seen, there is a discontinuity in profile a in Fig. 3, indicating that the order of terms in its Fourier series expansion is $\mathcal{O}(1/r)$. Profile b is continuous with discontinuities in its derivative, so that the expansion terms are $\mathcal{O}(1/r^2)$. The profile c is a modified square wave and is described by the equations

$$F(t) = \frac{G}{D^2}(3t^2 - 2t^3/D), \qquad 0 \le t \le D \tag{33a}$$

$$G, \qquad D \le t \le (T-D)/2 \tag{33b}$$

$$G\left\{1 - \frac{6}{D^2}[t-(T-D)/2]^2 + \frac{4}{D^3}[t-(T-D)/2]^3\right\}, \qquad \frac{T-D}{2} \le t \le \frac{T+D}{2} \tag{33c}$$

$$-G, \qquad \frac{T+D}{2} \le t \le T-D \tag{33d}$$

$$G\left\{-1 + \frac{3}{D^2}[t-(T-D)]^2 - \frac{2}{D^3}[t-(T-D)]^3\right\}, \qquad T-D \le t \le T \tag{33e}$$

where $G = AT^2/(T-D)^2$. Note that $F(t)$ is continuous with continuous derivatives,[13] so that the expansion terms are $\mathcal{O}(1/r^3)$. Profile d in Fig. 3 is a simple sinusoid, so that its expansion has only one nonzero term, which is $\mathcal{O}(1)$.

For each of the profiles we can calculate closed-form expressions for the response. We are particularly interested in the energy levels in the elastic modes at the end of the maneuver. Because there is no external excitation after the maneuver is over, the amplitude of the elastic motion after the maneuver depends on the energy level at $t = T$. Using the expression for the response given in Eq. (31), we calculate the modal energy as

$$E_r(t) = \tfrac{1}{2}[\dot{u}_r^2(t) + \omega_r^2 u_r^2(t)], \qquad r = 1,2,... \tag{34}$$

The energy levels at the end of the maneuver can be shown to be

$$E_r(T) = \frac{2A^2B_r^2}{\omega_r^2}[1 - \cos(\omega_r T/2)]^2 \tag{35a}$$

$$E_r(T) = \frac{32A^2B_r^2}{T^2\omega_r^4}\{10 - 8[\cos(\omega_r T/4) + \cos(\omega_r T/2) - \cos(3\omega_r T/4)] - 2\cos(\omega_r T)\} \tag{35b}$$

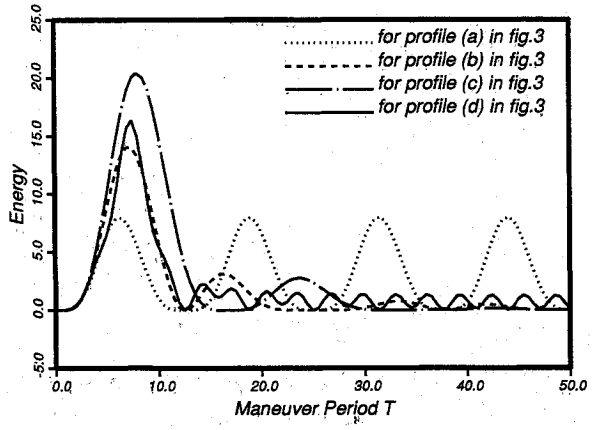

Fig. 4 Energy levels at $t = T$ for $\omega_r = 1$.

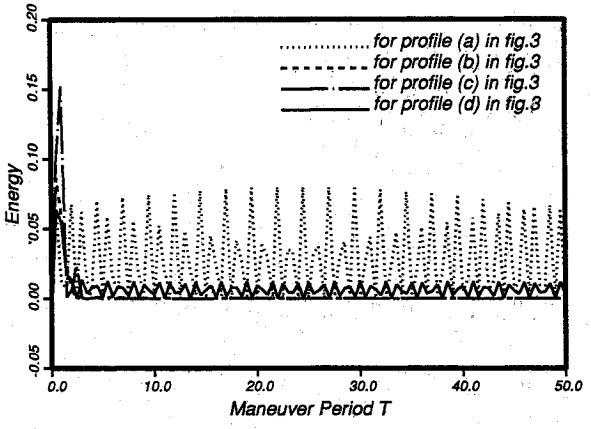

Fig. 5 Energy levels at $t = T$ for $\omega_r = 10$.

$$E_r(T) = \frac{\pi^2}{8}\frac{A^2B_r^2}{\omega^2 - \omega_r^2}[(\omega \sin\omega_r T - \omega_r \sin\omega T)^2 + \omega^2(\cos\omega_r T - \cos\omega T)^2], \qquad \omega = 2\pi/T \neq \omega_r \quad (35c)$$

for the profiles *a*, *b*, and *d* in Fig. 3, respectively. The equation for $E_r(T)$ for profile *c* in Fig. 3 is not given here because it is very lengthy.[14]

The values of $E_r(T)$ for $\omega_r = 1$ and $\omega_r = 10$ are plotted in Figs. 4 and 5, respectively, as a function of the maneuver period T. For the modified square wave, we use a ratio of $D = T/4$. Note that $\omega_r T$ can be used as a parameter while selecting the maneuver period T, except for profile *a* in Fig. 3. In all cases $E_r(T)$ shows oscillatory behavior. As expected, profile *a* in Fig. 3 gives the worst results, and the amplitude of oscillation decreases as the torque profile becomes smoother.

We observe from Figs. 4 and 5 that the sinusoidal excitation (profile *d*) yields energy levels that do not diminish beyond a particular level. This is because there always is only one term in the expansion of that torque profile, and the coefficient of that term is $\mathcal{O}(1)$. We also note that it is possible to select the maneuver period T so that the energy in a particular elastic mode is identically zero after the maneuver.[15] In general, though, one must consider the energy levels in all the modes that contribute to the motion.

Figure 6 plots the values of $E_r(T)$ for the modified square with varying magnitudes of D, the period during which the magnitude of the input changes rapidly. Selecting a larger value of D yields higher amplitudes for $E_r(T)$ for small values of the product $\omega_r(T)$, but lower amplitudes for other values of $\omega_r(T)$. Given a particular model and maneuver period, one can select a value for D using Fig. 6 that yields the lowest elastic motion amplitudes.

We conclude from the preceding observations that selection of the input profile should depend not only on the number of

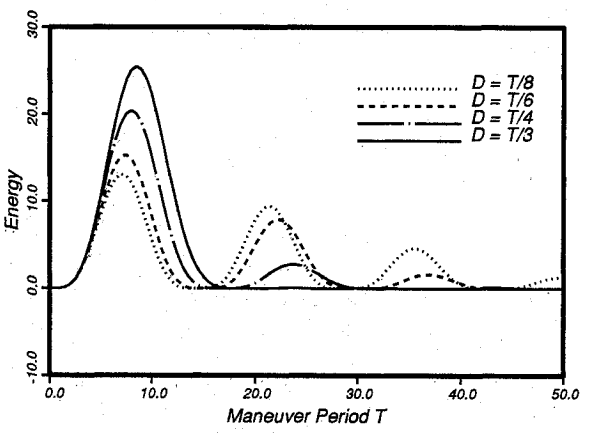

Fig. 6 Energy levels for the modified square wave.

times the profile is differentiable but also on the relationship between the natural frequencies ω_r and the maneuver period T.

V. Illustrative Examples

In this section we consider two types of structural control problems. The first deals with elastic motion suppression. The second deals with maneuver of a flexible body, where the elastic motion is not controlled.

The model considered for the first example is a simply supported uniform beam in bending, with unit mass and stiffness, and a length of $L = 10$. We consider modal control of the beam, retain eight modes in the model and control the first five, using a linear control law based on independent modal space control[9] that requires five actuators. We assume that a sufficient number of sensors is available to permit extraction of the modal coordinates from the system output with negligible error, and we compare the performances of the various actuation mechanisms.

The control method is based on selecting the gains at the modal level and then synthesizing the actual control inputs. We use a modal control law in the form

$$f_r(t) = \alpha_r u_r(t) + \beta_r \dot{u}_r(t), \qquad r = 1,2,\ldots,5 \quad (36)$$

where α_r amd β_r are modal feedback gains, selected as in Ref. 9. The relation between the input vector $\boldsymbol{F}(t)$ and the modal force vector $f_C(t) = [f_1(t)f_2(t)\cdots f_5(t)]^T$ is given by $f_C(t) = B\boldsymbol{F}(t)$, where the entries of B are defined in Eqs. (6–12) for the various types of actuators. We invert this relation and obtain the actual control input as in Ref. 9:

$$\boldsymbol{F}(t) = B^{-1} f_C(t) \quad (37)$$

For comparison purposes we select the same modal feedback gains for each type of actuator, so that the closed-loop poles of the system are the same. We give the beam an initial impulse at $x = 0.63L$ and calculate both the response and the work done by the actuators. The work done is defined for force actuators as

$$W = \int_0^T \int_0^L |f(x,t)\dot{u}(x,t)| \, dx \, dt \quad (38)$$

The absolute value signs are necessary to account for both positive and negative work. This is because the residual dynamics may alter the sign of the velocity and cause positive work to be done, even though the control action is intended to generate negative work only. Positive work in vibration suppression implies wasted energy and excitation of undesirable motion. As the residual mode amplitudes get smaller, less energy is expected to be wasted.[14]

For point forces, the work expression can be shown to be

$$W = \sum_{j=1}^{m} \int_0^T |F_j(t)\dot{u}(x_{aj},t)|\,dt \tag{39}$$

and for piecewise-continuous actuators the work expression becomes

$$W = \sum_{i=1}^{m} \int_0^T \int_{x_{ai}-\varepsilon}^{x_{ai}+\varepsilon} \left|\frac{F_i(t)}{2\varepsilon}\dot{u}(x,t)\right| dx\,dt \tag{40}$$

which is based on the assumption that the entire length of the actuator is in contact with the beam at all times. Similarly, for point torquers we have

$$W = \sum_{j=1}^{m} \int_0^T |M_j(t)\dot{u}'(x_{tj},t)|\,dt \tag{41}$$

We select the actuators locations as $x_{ai} = x_{ti} = 0.11L$, $0.33L$, $0.48L$, $0.68L$, $0.87L$, and the final time as $T = 40$ s. The system is excited with an impulsive force, from which the initial energy level is calculated using Eq. (34) as 0.40. Table 1 shows the work done by the point force and torque actuators and by the piecewise-continuous force actuators for varying values of the contact length 2ε. To make the example more realistic, we also compare the results after adding modal damping of $\zeta = 0.02$ to the system equations.

We observe that the piecewise-continuous and point force actuators do comparable amounts of work, and torque actuators give the worst results. Even though one expects piecewise-continuous actuators to perform better, we can explain the near-identical performance by noting that the force density of the piecewise-continuous actuators is the same throughout the contact length. If there is a sign change in the velocity within the contact length of the actuator, the piecewise-continuous controller performs both negative and positive work at the same time. This raises the issue of determining the optimal number, location, and size of piecewise-continuous actuators, which we will be investigating in a forthcoming publication. It should also be noted that the amplitudes of the control inputs differ when point and piecewise-continuous actuators are used.

It was also observed from response simulations that point torques are much more sensitive to the distribution of the actuators along the beam than point forces. This can be explained by noting that, whereas each eigenfunction $\phi_i(x)$ has $i-1$ nodes (or nodal lines) for the ith mode ($i = 1,2,...$), the slopes of the eigenfunctions $\phi_i'(x)$ have i nodes for the ith mode.

Table 1 Comparison of work

	$\zeta = 0$	$\zeta = 0.02$
Point force	0.3808	0.2670
$2\varepsilon = 0.1$	0.3806	0.2674
$2\varepsilon = 0.3$	0.3820	0.2696
Torque	1.6159	0.9303

We next consider a decentralized control law of the form $F_j(t) = \alpha_j' u(x_{aj},t) + \beta_j' \dot{u}(x_{aj},t)$, ($j = 1,2,...,m$), in which α_j' and β_j' ($j = 1,2,...,m$) are feedback control gains, for both point actuators and for piecewise-continuous actuators. We use the same actuator locations as those in the previous example and select the control gains as $\alpha_j' = 0.0$, $\beta_j' = -0.4$ ($j = 1,2,...,5$). The closed-loop poles are obtained by solving the associated eigenvalue problem.

Table 2 compares the closed-loop poles using a model consisting of eight modes. For the point force case the real parts of the closed-loop poles remain at about the same magnitude, but magnitudes of their real parts decrease when piecewise-continuous actuators are used and as the contact length is increased. This is another indication that the higher modes receive less control when piecewise-continuous actuators are used. We also observe that, if the contact lengths of the piecewise-continuous actuators are increased, the highest modes can become unstable, for the same reason cited earlier with respect to performing both positive and negative work at the same time.

As suggested earlier, one way of approaching smoothness in the excitation profile is by increasing the number of actuators. To investigate this issue, we consider a torque acting on a free-free beam. The dimensions and material properties of the beam are taken as the same as in Ref. 16. The torque is realized by couples of point forces. Denoting the beam length by L and placing the origin of the coordinate system at the midpoint, the actuator locations are selected as

$$x_{ai} = \pm\frac{L}{2}\frac{i}{m/2+1}, \qquad i = 1,2,...,m/2 \tag{42}$$

The forces $\pm F_i$ act at locations $\mp x_i$ ($i = 1,2,...,m/2$). The total moment is given by

$$M = \sum_{i=1}^{m/2} 2F_i|x_{ai}| \tag{43}$$

We select force amplitudes as $F_i = F$, such that $F = M/\Delta_m$, in which

$$\Delta_m = \sum_{i=1}^{m/2} 2|x_{ai}| \tag{44}$$

It follows from Eq. (6) that the modal forces have the form

$$f_r = F\sum_{i=1}^{m/2}[\phi_r(-x_{ai}) - \phi_r(x_{ai})], \qquad r = 3,4,... \tag{45}$$

Because of the symmetry of the eigenfunctions and of the actuator locations, the odd modes are not affected by the excitation. Table 3 compares the values of f_r for the second and fourth elastic modes and for varying numbers of actuators. It is clear that increasing the number of actuators results in less excitation of the elastic motion.

In the second example we consider maneuver of a pinned-free bar shown in Fig. 7. The dimensions and material properties of the link are taken as the same as those in the previous

Table 2 Closed-loop poles for decentralized control

Point force		$\varepsilon = 0.4020$		$\varepsilon = 1.2020$	
−0.0839	0.0000	−0.0854	0.0000	−0.0976	$\pm j$0.0144
−0.1161	0.0000	−0.1141	0.0000		
−0.1001	$\pm j$0.3821	−0.0990	$\pm j$0.3823	−0.0908	$\pm j$0.3842
−0.1002	$\pm j$0.8834	−0.0978	$\pm j$0.8835	−0.0800	$\pm j$0.8848
−0.1004	$\pm j$1.5791	−0.0961	$\pm j$1.5789	−0.0661	$\pm j$1.5784
−0.2000	$\pm j$2.4593	−0.1870	$\pm j$2.4603	−0.1006	$\pm j$2.4653
−0.0996	$\pm j$3.5446	−0.0904	$\pm j$3.5458	−0.0338	$\pm j$3.5513
−0.0998	$\pm j$4.8308	−0.0873	$\pm j$4.8317	−0.0181	$\pm j$4.8355
−0.0999	$\pm j$6.3126	−0.0838	$\pm j$6.3134	−0.0040	$\pm j$6.3164

Table 3 Modal forces for varying numbers of actuators

No. of actuators	f_4	f_6
2	0.3199	0.1398
4	0.2415	0.0481
6	0.2066	0.0201
8	0.1867	0.0065

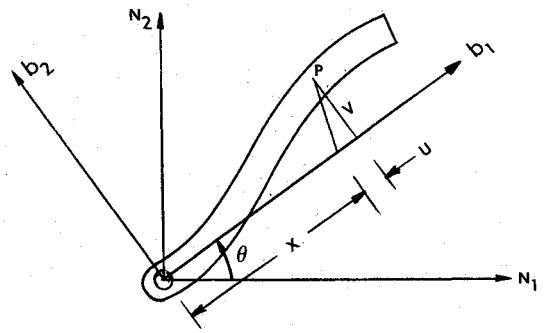

Fig. 7 The pinned-free link.

example. The actuation mechanism is a torquer located at the pin joint. The first natural frequency associated with the linear small-motions model is 15.3 rad/s.

A set of body-fixed coordinates $b_1b_2b_3$ is used to describe the elastic motion. The body axes are obtained by rotating the inertial coordinates by angle θ, so that the elastic deformation $u(x,t)$ measured from the body-fixed frame will have no rigid-body component.[16]

The orientation of a point x on the beam after deformation is given by

$$\boldsymbol{r}(x,t) = [x + v(x,t)]\boldsymbol{b}_1 + u(x,t)\boldsymbol{b}_2 \tag{46}$$

in which $u(x,t)$ is the transverse deformation and $v(x,t)$ is the stretch. The elastic deformation $u(x,t)$ is expanded as

$$u(x,t) = \sum_{i=1}^{n} \psi_i(x)u_i(t) \tag{47}$$

where n is the order of the expansion, $\psi_i(x)$ are trial functions, and $u_i(t)$ are their coefficients. The mathematical model is obtained by considering the large-angle rigid-body motion together with centrifugal stiffening. Details of the derivation can be found in Ref. 16. The equations of motion become, for the rigid-body mode,

$$\left\{I + \sum_j \sum_i \left[m_{ij} - h_{ij}\right]u_i(t)u_j(t)\right\}\ddot{\theta}(t) + 2\sum_j \sum_i \left[m_{ij} - h_{ij}\right]u_i(t)\dot{u}_j(t)\dot{\theta}(t) = M(t) \tag{48}$$

and, for the elastic modes,

$$\sum_j \left\{m_{ij}\ddot{u}_j(t) + \left(k_{ij} + [h_{ij} - m_{ij}]\dot{\theta}^2(t)\right)u_j(t)\right\} = f_i(t) \qquad i = 1,2,\ldots \tag{49}$$

in which I is the mass moment of inertia of the undeformed link about the pin joint, $m_{ij} = [\psi_i(x), m(x)\psi_j(x)]$, $k_{ij} = [\psi_i(x), EI(x)\phi_j''''(x)]$, and h_{ij} describe the centrifugal stiffening effect, which can be shown to have the form[16]

$$h_{ij} = \int_0^L x \int_0^x \psi_i'(y)\psi_j'(y)\,dy\,dx \tag{50}$$

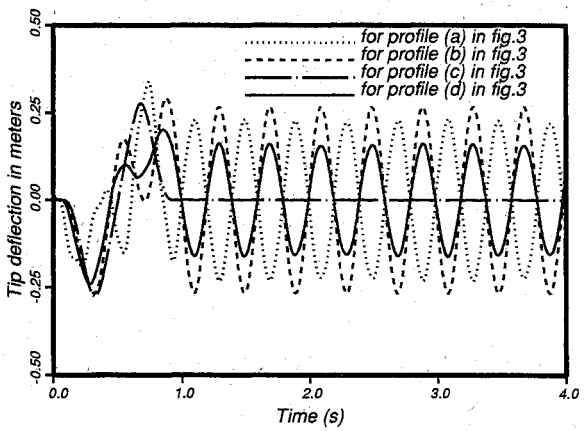

Fig. 8 Elastic deformation of free end for $T = 1$ s.

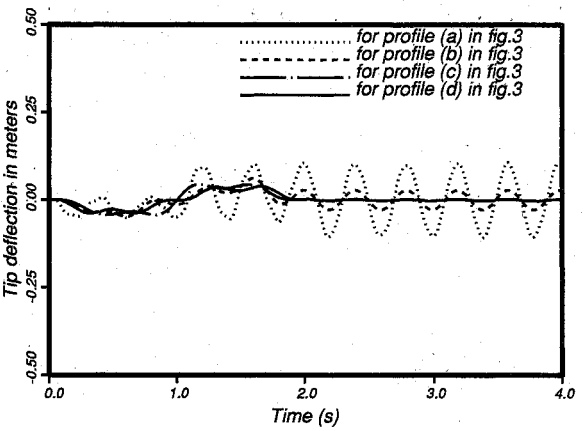

Fig. 9 Elastic deformation of free end for $T = 2$ s.

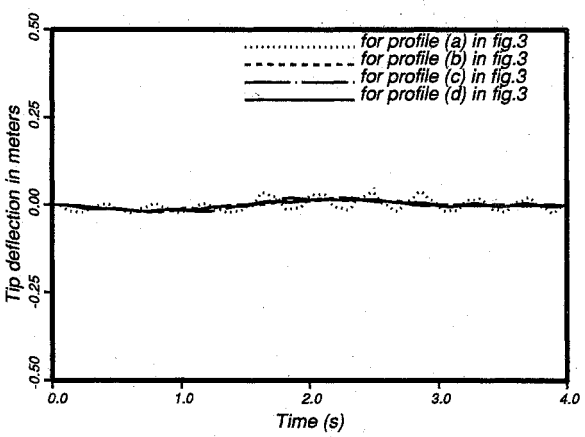

Fig. 10 Elastic deformation of free end for $T = 3$ s.

$M(t)$ is the applied torque, and $f_i(t)$ is the excitation the elastic motion receives due to the discrete torque in the form $f_i(t) = M(t)\phi_i'(0)$ [Eqs. (11) and (12)]. We use as expansion functions the eigenfunctions of the bar, which results in $m_{ij} = \delta_{ij}$, $k_{ij} = \omega_j^2\delta_{ij}$ $(i,j = 1,2,...)$, where ω_j are the natural frequencies associated with the linear model.

We perform a rest-to-rest maneuver of the robot arm and apply torques whose profiles are given in Fig. 3. We compare the elastic motion amplitudes at the tip of the beam using two elastic modes in the model. As stated earlier, the torque levels are selected so that, in the event of no elastic motion, the final position of the beam would be the same. Figures 8–10 plot the elastic motion amplitudes for maneuver periods of 1–3 s, respectively. As expected, the smoother torque profiles excite the elastic motion less. Also, the maneuver period is very much related to the elastic motion amplitude; thus, selection of the

profile should depend on the smoothness of the profile, the maneuver period, and the natural frequencies associated with the elastic motion.

VI. Conclusions

The existence of the Gibbs effect during control of flexible structures is investigated. It is shown that, if point or piecewise-continuous controllers are used, discontinuities exist in the spatial distribution of the control profile. These discontinuities lead to the Gibbs effect when the control profile is expanded spatially. The consequence of having the Gibbs effect is the excitation of undesirable motion. An analysis of the response amplitudes indicates that, among discrete controllers, piecewise-continuous force controllers are the most desirable and point torquers the least. The Gibbs effect may also be present in the Fourier series expansion of the temporal profile of the control action, leading to higher amplitudes and energy levels in the elastic motion. The time histories of various rigid-body maneuvers are compared with respect to how much they excite the elastic motion. It is recommended that both the spatial and temporal distributions of the control input be selected so that they are as smooth as possible.

References

[1]Kufner, A., and Kadlec, J., *Fourier Series*, Iliffe, London, 1971.

[2]Lanczos, C., *Discourse on Fourier Series*, Oliver & Boyd, Edinburgh, Scotland, UK, 1966.

[3]Gottlieb, D., and Orszag, S. A., *Numerical Analysis of Spectral Methods: Theory and Applications*, Society for Industrial and Applied Mathematics, Arrowsmith, Bristol, England, UK, 1977.

[4]Tadikonda, S. S. K., and Baruh, H., "Gibbs Phenomenon in Structural Mechanics," *Proceedings of the 30th AIAA Structures, Structural Dynamics, and Materials Conference*, AIAA, Washington, DC, 1989, pp. 337–347.

[5]Baruh, H., and Tadikonda, S. S. K., "Another Look at Admissible Functions," *Journal of Sound and Vibration*, Vol. 132. No. 1, 1989, pp. 73–87.

[6]Öz, H., "Control of Flexible Systems and Principles of Structural Mechanics," AIAA Paper 84-2001, Aug. 1984.

[7]Silverberg, L. M., and Baruh, H., "Simulations Maneuver and Vibration Suppression of Flexible Spacecraft," *Applied Mathematical Modelling*, Vol. 12, Dec. 1988, pp. 546–555.

[8]Greenberg, M. D., *Foundations of Applied Mathematics*, Prentice-Hall, Englewook Cliffs, NJ, 1978.

[9]Meirovitch, L., and Baruh, H., "Control of Self-Adjoint Distributed-Parameter Systems," *Journal of Guidance, Control, and Dynamics*, Vol. 5, No. 1, 1982, pp. 60–66.

[10]Courant, R., and Hilbert, D., *Methods of Mathematical Physics*, Vol. 1, Wiley-Interscience, New York, 1953.

[11]Meirovitch, L., and Silverberg, L. M., "Globally Optimal Control of Distributed-Parameter Systems," *Optimal Control Applications and Methods*, Vol. 4, 1983, pp. 365–386.

[12]Lee, C.-K, Chang, W.-W., and O'Sullivan, T. C., "Piezoelectric Modal Sensors and Actuators Achieving Active Damping on a Cantilever Plate," *Proceedings of the 30th AIAA Structures, Structural Dynamics, and Materials Conference*, AIAA, New York, 1988, pp. 2018–2026.

[13]Junkins, J. L., "Near Minimum-Time Feedback Control of Distributed Systems: A Liapunov Design Method," *Proceedings of the Seventh VPI&SU Symposium on Dynamics and Control of Large Structures*, edited by Z. Rahman, H. Bang, and N. Hecht, Virginia Polytechnic Inst. and State Univ., Blacksburg, VA, May 1989, pp. 637–652.

[14]Tadikonda, S. S. K., "Modeling and Control of Flexible Manipulators and Associated Computational Issues in Mechanics," PhD Dissertation, Rutgers, New Brunswick, NJ, Oct. 1989.

[15]Akulenko, L. D., and Bolotnik, N. N., "On Rotation Control of an Elastic Link Manipulator," *Engineering Cybernetics*, Vol. 22, No. 2, 1984, pp. 108–113.

[16]Baruh, H., and Tadikonda, S. S. K., "Issues in the Dynamics and Control of Flexible Robot Manipulators," *Journal of Guidance, Control, and Dynamics*, Vol. 12, No. 5, 1989, pp. 659–671.